inorganics

MDPI

Article

Synthesis, Crystal Structure, Hirshfeld Surfaces Analysis, Interaction with DNA and Comparation of Different Bases in Hirshfeld Atom Refinement of New Polymorph of Chlorido(η^6-p-cymene)(diclofenac)Ruthenium(II) Organometallic Compound

Martin Schoeller [1], Milan Piroš [1], Karol Lušpai [2], Jana Braniša [3] and Ján Moncol [1,3,*]

[1] Department of Inorganic Chemistry, Slovak University of Technology, Radlinského 9, 812 37 Bratislava, Slovakia; martin.schoeller@stuba.sk (M.S.)
[2] Department of Physical Chemistry, Slovak University of Technology, Radlinského 9, 812 37 Bratislava, Slovakia
[3] Department of Chemistry, Faculty of Natural Sciences, Constatine the Philosopher University in Nitra, 949 74 Nitra, Slovakia
* Correspondence: jan.moncol@stuba.sk

Abstract: A new polymorph of the ruthenium(II) diclofenac complex with formula [Ru(p-cymene)(diclo)Cl] was synthesized, and its crystal structure was solved by single crystal X-ray diffraction. The structure was refined by HAR, using five different relativistic bases sets (x2c-SVP, jorge-DZP-DKH, jorge-TZP-DKH, x2c-TZVP, and x2c-TZVPP) and three effective core potential basis sets (ECP-def2-SVP, ECP-def2-TZVP, and ECP-def2-TZVPP). Their influence on the structure parameters was compared. The analysis of the supramolecular structure of the HAR/non-HAR structures, as well as of the orthorhombic polymorph, was supported by the calculation and analysis of the Hirshfeld surfaces. The best results were observed for HAR using triple-zeta-based sets. No significant effect of base choice on Hirshfeld surfaces was observed. A study of the ability of the complex to interact with ct-DNA was also performed. The complex was shown to interact with ct-DNA, but the mode of interaction is not fully elucidated.

Keywords: crystal structure; HAR; ruthenium(II); NSAID; diclofenac; biological activity

Citation: Schoeller, M.; Piroš, M.; Lušpai, K.; Braniša, J.; Moncol, J. Synthesis, Crystal Structure, Hirshfeld Surfaces Analysis, Interaction with DNA and Comparation of Different Bases in Hirshfeld Atom Refinement of New Polymorph of Chlorido(η^6-p-cymene)(diclofenac)Ruthenium(II) Organometallic Compound. *Inorganics* **2023**, *11*, 190. https://doi.org/10.3390/inorganics11050190

Academic Editor: Hristo P. Varbanov

Received: 13 March 2023
Revised: 27 March 2023
Accepted: 31 March 2023
Published: 27 April 2023

1. Introduction

Diclofenac (diclo) is one of the most prescribed non-steroidal anti-inflammatory drugs (NSAID) in the world. In addition to its anti-inflammatory effects, it is also indicated for its analgesic and antipyretic effects. The mechanism of action of diclofenac, similar to other NSAIDs, is based on the suppression of the conversion of arachidonic acid to prostaglandin via the inhibition of cyclooxygenases (COX) [1,2]. There are three types of COX. The function of COX-1 is mainly associated with physiological functions such as the regulation of renal blood flow, gastric mucosal circulation, proper thrombocyte function, etc. On the other hand, COX-2 is activated during inflammatory processes and is involved in tumor invasion and metastasis [3,4]. Side effects of NSAIDs are mostly associated with a lack of selectivity of COX-2 inhibition [3]. Several papers have been published showing that transition metal complexes with NSAIDs have enhanced anti-inflammatory activity, reduced side effects, and several of them exhibit cytostatic, cytotoxic, and anti-neoplastic effects [5,6].

Several structures of metal complexes in which diclofenac acts as a ligand have been published in Cambridge Structure Database (CSD) so far [7–26]. Almost in all complexes, diclofenac coordinates via the carboxylic group (coordination via the chlorine atom has also

been observed). However, only seven coordination modes of this ligand were observed. A very common mode of coordination is the terminal monodentate, in which diclofenac binds via a single oxygen atom to a central atom. Another common mode of coordination is the chelate mode, in which both oxygen atoms are bonded to one central atom. Two modes of coordination in which the two central atoms are bridged were observed, namely, *syn-anti* and *syn-syn* (Figure 1). The *syn-syn* mode is observed in complexes whose central atoms have short internuclear spacing. For example, in silver(I) complexes, such as $[Ag_2(diclo)_2(\gamma\text{-pic})_2]$ (γ-pic = 4-methylpyridine) (CSD Refcode CEVGOC) [27] and "paddle wheel" copper(II) complexes such as $[Cu_2(diclo)_4(MeOH)_2]$ (MeOH = methanol) (CSD Refcode QIWXEC) [28] or $[Cu_2(diclo)_4(DMSO)_2]$ (DMSO = dimethyl sulfoxide) (CSD Refcode YAVBUU) [29]. *Syn-anti* mode of coordination is less common and was described in the case of the organometallic tin(IV) compound with formula *catena*-poly-$[Sn(CH_3)_3(diclo)]$ (CSD Refcode WAPGUT) [30]. Another way to bridge two central atoms is through a single carboxylate oxygen atom. This mode of coordination is observed in the case of $[Sn_4(Bu)_8(diclo)_4]$ (Bu = butyl(1-))(CSD Refcode KALYIF) [31]. The structures in which diclofenac coordinates to one central atom in a bidentate chelating manner and at the same time one of the oxygen atoms coordinates to the other central atom (μ^2-η^2:η^1 chelating + bridging mode) (Figure 1) have also been published, for example, in case of complex $[Cd(diclo)_2]$ (CSD Refcode UXOVUA) [32]. The mode of coordination in which diclofenac bridges up to three central atoms was also described in *catena*-$[Ag_4(\alpha\text{-pic})_3(diclo)_4]$ (α-pic = 2-methylpyridine) (CSD Refcode CEVGUI) [27].

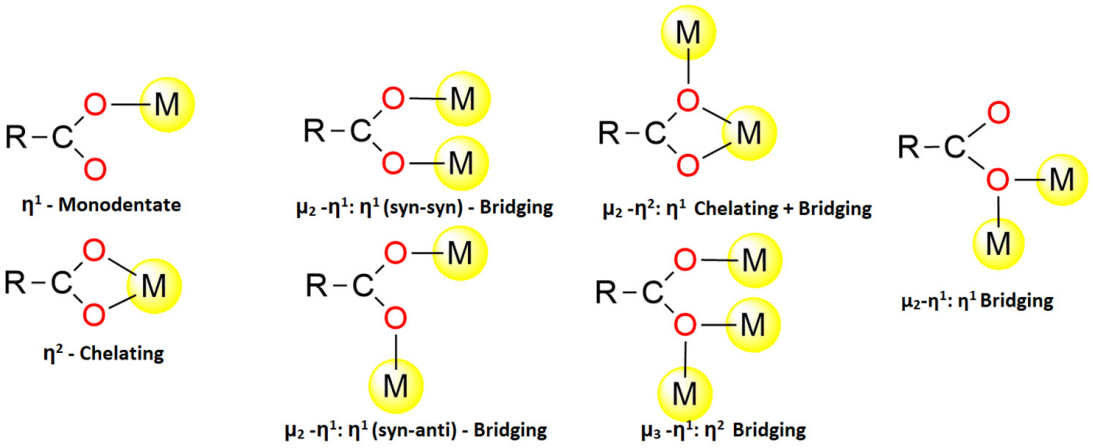

Figure 1. Most common modes of diclofenac ligand coordination.

Oliviera et al. studied the biological activity of a series of four ruthenium(II) complexes whose composition can be described by the formula [Ru(bipy)(diclo)L] (L = dppe–1,2-bis(diphenylphosphino)ethane, dppp–1,3-bis(diphenylphosphino)propane, dppb–1,4-bis(diphenylphosphino)butane, or dppf–1,1'-bis(diphenylphosphino)ferrocene). All complexes were shown to exhibit higher cytotoxicity compared to cisplatin and diclofenac alone against the A549 (lung cancer), MDA-MB-231 (epithelial breast cancer), MCF-7 (breast cancer), MRC-5 (non-tumor human lung fibroblast cells), and MCF-10A (non-tumor breast cells) cell lines. The complexes show significant affinity to interact with bovine serum albumin (BSA), and a study of the interaction with calf-thymus DNA (ct-DNA) demonstrated minor groove binding [33]. Khan et al. published a study of the biological activity of a complex whose molecular structure obtained by indirect methods can be described by the formula [Ru(p-cymene)(diclo)(DMSO)Cl]. The synthesis of this complex is based on the reaction of the dimeric precursor $[Ru_2(p\text{-cymene})_2Cl_4]$ with sodium diclofenac salt in dry methanol with a few drops of dimethyl sulfoxide at 80 °C for ten hours. Based on the infrared spectrum, diclofenac is coordinated in a chelating manner. The interaction with ct-DNA was also studied by UV-Vis spectroscopy and by studying the ability to displace ethidium bromide (EB) from the EB–DNA complex. Complex interacts with

DNA via intercalation and minor groove binding. The apparent association constant is found to be 1.85×10^4 M^{-1}. The cytotoxic effect on the MCF-7 cell line is comparable to cisplatin [34]. Mandal et al. published a series of three ruthenium complexes with different NSAIDs, the composition of which is described by the formulae [Ru(p-cymene)(nap)Cl], [Ru(p-cymene)(diclo)Cl], and [Ru(p-cymene)(ibu)Cl] (nap = naproxen, diclo = diclofenac and ibu = ibuprofen). Complex with diclofenac was prepared by reacting the dimeric precursor with the sodium salt of diclofenac in a mixed solvent (methanol–dichloromethane). Crystals suitable for single crystal X-ray crystallography were prepared by diffusion of diethyl ether into dichloromethane (DCM) solution. Ru(p-cymene)(diclo)Cl] crystallizes in an orthorhombic crystal system with the *P*bca space group. The complex exhibits significant antiproliferative activity against A549, MCF7, and HeLa (cervical cancer) cell lines. The complex was also shown to be able to inhibit COX. From the study of the stability of the complexes, the authors point out that the complexes can only act as pro-drugs, and the structure of the active form is still unknown [35]. The primary aim of this paper is to present the effect of the choice of bases set at HAR on the crystallographic parameters. The polymorph of the complex, which has been previously published (different polymorph), was used as the object of research on this influence. This polymorph was prepared by modifying the crystallization conditions. As a secondary aim of the work, the already published study of the interaction of this complex with DNA is complemented by a study using UV-Vis titration.

2. Results

2.1. Synthesis and Spectral Properties

The procedure for preparing the single crystal of the polymorph published here (triclinic, $P\bar{1}$) is slightly different from the method published previously (orthorhombic polymorph, *P*bca). The main difference was that the single crystals were prepared in a refrigerator after the addition of diethyl ether. The orthorhombic polymorph was prepared by the diffusion method. Another difference is the temperature at which the X-ray data were collected. The dataset of triclinic polymorph was collected at 100 K; otherwise, the orthorhombic were collected at 298 K [35].

The ^{1}H NMR spectrum of the prepared complex is presented in Figure S1 (Supplementary Material). The highest chemical shifts have ring protons of diclofenac ligand, specifically multiplet peaks in the area from 6.50 ppm to 7.32 ppm. In the range of 5.39 ppm–5.60 ppm, we can observe two characteristic doublet signals of p-cymene aromatic ring protons. The singlet, at 3.54 ppm with the integral intensity corresponding to two protons, can be assigned to the -CH_2-COO group of the diclofenac ligand. The multiplet peak at 2.86 ppm belongs to the -$CH(CH_3)_2$ group of isopropyl-part of the p-cymene ligand. The peak of the methyl-substituent of p-cymene is observed as a singlet at 2.27 ppm. The two methyl groups of isopropyl substituents -$CH(CH_3)_2$ have the lowest chemical shifts, concretely, 1.29 ppm. The signals belonging to protons of used solvents can also be found in the spectrum. The spectrum is complicated by several proton signals of low integral intensity, which can be attributed to the partial hydrolysis of the complex, as previously observed in similar complexes [14]. For this reason, the solution of the complex for ct-DNA titrations was always prepared only prior to measurement.

The infrared spectrum (Figures S2–S4 in Supplementary Material) agrees with structural information obtained by single-crystal X-ray diffraction. The band at 3286 cm^{-1} can be attributed to valence vibrations ν(NH) of the secondary amine group of the diclofenac ligand. The presence of only one band in this region confirms that in the solid state, this group is not hydrogen bonded. Valence vibrations ν(CH) of aromatic groups can be found at 3066 cm^{-1}. The presence of methyl groups can be observed on the asymmetric valence vibrations band at 2956 cm^{-1}, and symmetric vibrations are observed at 2864 cm^{-1}. The band at 1191 cm^{-1} can be assigned to skeletal vibrations of -CH-$(CH_3)_2$. These bands, thus, provide strong evidence for the presence of p-cymene. The very intensive band at 776 cm^{-1} corresponds to deformational vibrations γ(CCH) of four neighboring C–H bonds

of aromatic rings. Bands corresponding to $\nu_{as}(COO^-)$ and $\nu_s(COO^-)$ occur at 1506 cm^{-1} and 1442 cm^{-1}. The difference between these two bands (δ) is lower than 150 cm^{-1} (specifically δ = 64 cm^{-1}), which is consistent with the bidentate chelate mode of coordination of diclofenac [36].

2.2. Crystal Structure

The molecular structure of the prepared complex is shown in Figure 2. Complex crystallizes in a triclinic system with centrosymmetric space group $P\bar{1}$. The coordination number of the ruthenium(II) central atom can be quantified by the number nine. The geometry of the coordinating polyhedron is pseudo-octahedral, with three octahedral sites occupied by p-cymene. The two coordination sites are occupied by oxygen-donor atoms of the carboxylic group of diclofenac. Thus, diclofenac acts as bidentate chelate ligand. The corresponding bond lengths are *d*(Ru-O1) = 2.1412(16) Å and *d*(Ru-O2) = 2.1706(16) Å. The p-cymene ligand is coordinated with the central atom in a η^6-manner. The complex can be described as a half-sandwich or piano-stool complex. The last coordination site on the ruthenium(II) is occupied by the chlorido ligand. The bond length is *d*(Ru-Cl1) = 2.3826(6) Å. Selected bond lengths are summarized in Table 1 with regard to the HAR method of refinement used.

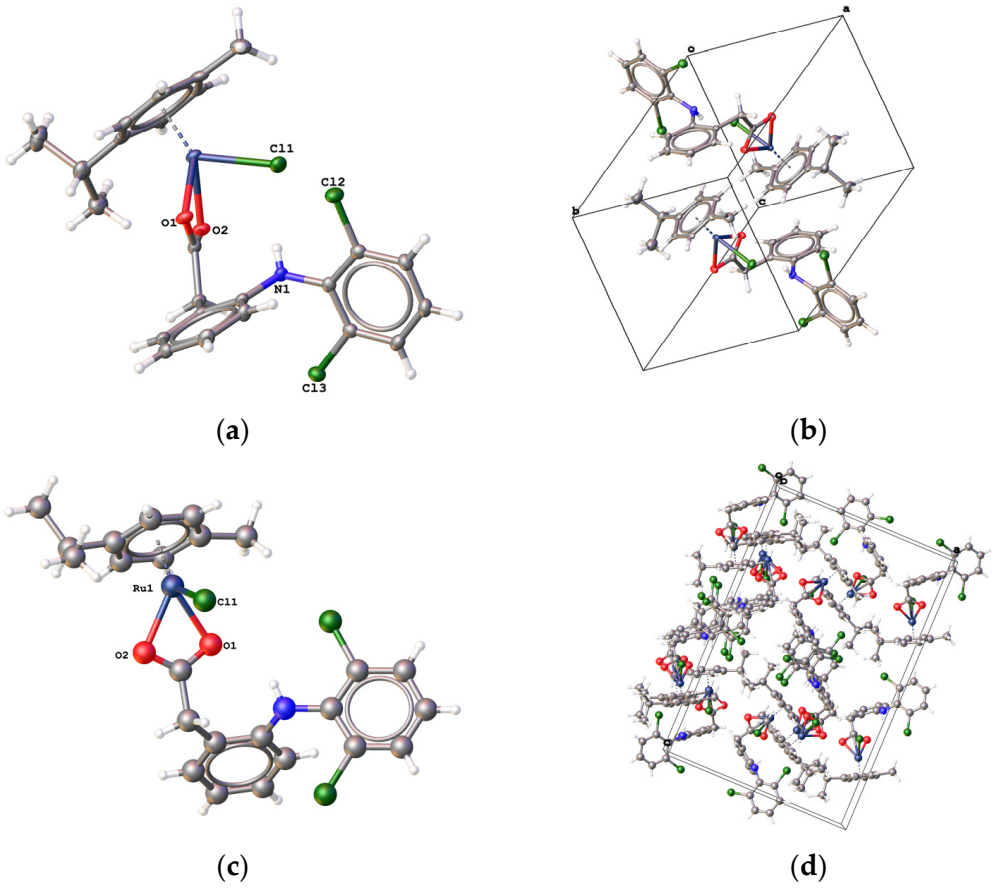

Figure 2. ORTEP style figure of molecular structure of complex 1 (**a**); packing of this complex in unit cell (**b**); molecular structure of published orthorhombic polymorph [Ru(p-cymene)(diclo)Cl] (**c**); packing of this polymorph in unit cell (**d**).

Table 1. Comparison of HAR methods and IAM refinement on crystal structure parameters.

	1	**1a**	**1b**	**1c**	**1d**	**1e**	**1f**	**1g**	**1h**
Base set	IAM	x2c-SVP	Jorge-DZP-DKH	Jorge-TZP-DKH	x2c-TZVP	x2c-TZVPP	ECP-def2-SVP	ECP-def2-TZVP	ECP-def2-TZVPP
R_1 [$I \geq 2\sigma(I)$]	0.0226	0.0187	0.0195	0.0186	0.0186	0.0186	0.0185	0.0183	0.0183
wR_2 [$I \geq 2\sigma(I)$]	0.0616	0.0496	0.0511	0.0492	0.0492	0.0493	0.0492	0.0484	0.0484
R_1 [all data]	0.0244	0.0205	0.0212	0.0203	0.0203	0.0203	0.0202	0.0200	0.0200
wR_2 [all data]	0.0628	0.0506	0.0521	0.0501	0.0501	0.0502	0.0502	0.0494	0.0493
Ru1-Cl1	2.3820(6)	2.3816(5)	2.3816(5)	2.3817(5)	2.3817(5)	2.3817(5)	2.3817(5)	2.3817(5)	2.3817(5)
Ru1-O1	2.1711(15)	2.1705(12)	2.1709(12)	2.1705(12)	2.1705(12)	2.1705(12)	2.1702(12)	2.1702(12)	2.1702(12)
Ru1-O2	2.1434(15)	2.1425(12)	2.1429(12)	2.1426(12)	2.1426(12)	2.1426(12)	2.1422(12)	2.1422(12)	2.1422(12)
GOF	1.051	1.088	1.089	1.106	1.106	1.108	1.089	1.094	1.094
Largest difference peak/hole	1.18/−0.61	1.11/−0.69	1.10/−0.70	1.12/−0.69	1.13/−0.68	1.13/−0.69	1.12/−0.66	1.13/−0.66	1.13/−0.67

Based on the geometrical analysis in Olex2, no significant hydrogen bonds or π-π stacking interactions [37] are found in the supramolecular structure of this complex. On the other hand, the supramolecular structure of the orthorhombic polymorph [35] is stabilized by two types of π-π stacking interactions. Specifically, between two symmetrically equivalent chloride-substituted benzene rings of the diclofenac (∢ 9.284°; *d*(centroid···centroid) = 3.650 Å; shift = 1.348 Å). Another type of the π-π stacking interactions [37] is between the p-cymene and the arene ring of diclofenac (∢ 0°; *d*(centroid···centroid) = 3.624 Å; shift = 0.825 Å).

2.3. Hirshfeld Surfaces Analysis

The intermolecular interactions of the complex published here (triclinic polymorph, $P\bar{1}$), the complex previously published by Mandal et al. [35], and models obtained by HAR were analyzed by Hirshfeld surfaces which have been mapped over d_{norm} and shape index. Figure 3 shows Hirshfeld surfaces of a triclinic complex with Cl···H/H···Cl (d) and O···H/H···O (b); close contact is displayed with corresponding finger-plot (c, e). Figure 4 shows two views (a, b) on the Hirshfeld surface of orthorhombic polymorph depicted Cl···H/H···Cl close contacts with corresponding finger-plot prints (c). A significant difference can be observed on the surfaces, namely, in the number and positions of intense red areas (where are closer intermolecular contacts than the sum of van der Waals radii). These red areas represent mainly weak hydrogen bonds of C–H···X (where X = O, Cl) type. A lower number of these red areas is observed only for the orthorhombic polymorph. Consistent with the analysis in Olex2, no other intermolecular interactions present in the supramolecular structures of the complexes were found. Similarly consistent with the Olex2 geometric analysis is the observation of the complementary triangular surfaces with opposite signs of shape index in the case of orthorhombic polymorph, which is characteristic of the presence of the π-π stacking interactions. These alternating triangular patches were not observed in the case of triclinic polymorph nor in its HAR models. The Hirshfeld surfaces for other structures are presented in the supplementary material (Figures S5–S14). A view of the threedimensional Hirshfeld surface plotted over electrostatic potentials of IAM models of both polymorphs is shown in Figure S15. The electrostatic potential over the Hirshfeld surfaces is plotted; the blue region (positive electrostatic potential) over the surface represents the hydrogen donor potential, whereas the hydrogen bond acceptors (chlorine and oxygen atoms) are represented by the red region (negative electrostatic potential) [38]. The electrostatic potentials on the Hirshfeld surfaces of both polymorphs are very similar and correspond to hydrogen bonds of C–H···X (where X = O, Cl) type.

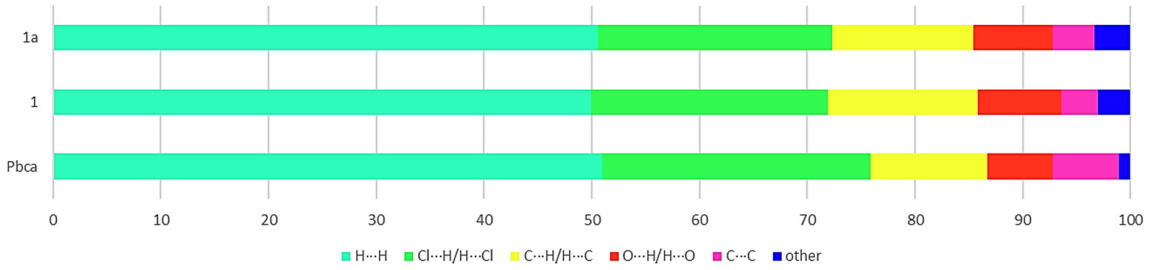

(**a**)

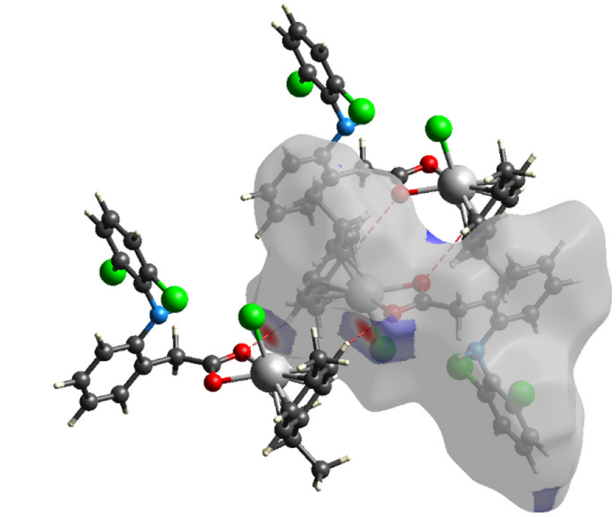

(**b**)

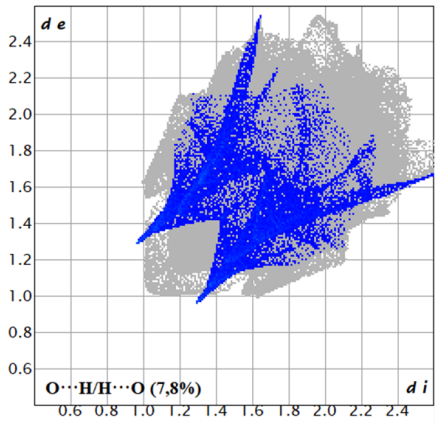

(**c**)

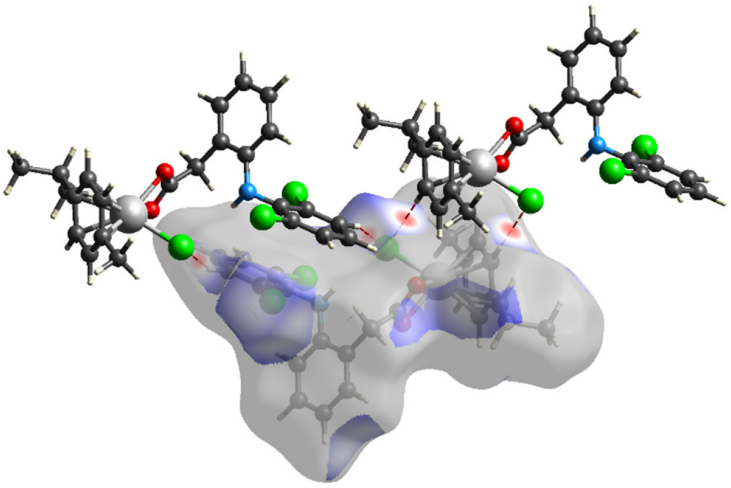

(**d**)

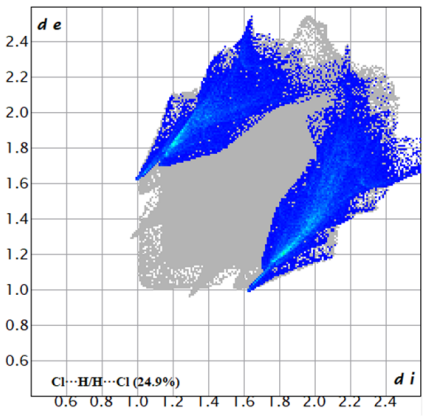

(**e**)

Figure 3. Graph showing the fraction of individual close contacts on the Hirshfeld surfaces for HAR model (1a), IAM model (1), and published polymorph (*P*bca) (**a**), d_{norm} mapped Hirshfeld surface of the IAM model of complex (**b**) with corresponding fingerprint plot showing only H· · ·O/O· · ·H close contacts (**c**), and Cl· · ·H/H· · ·Cl close contacts (**d**,**e**).

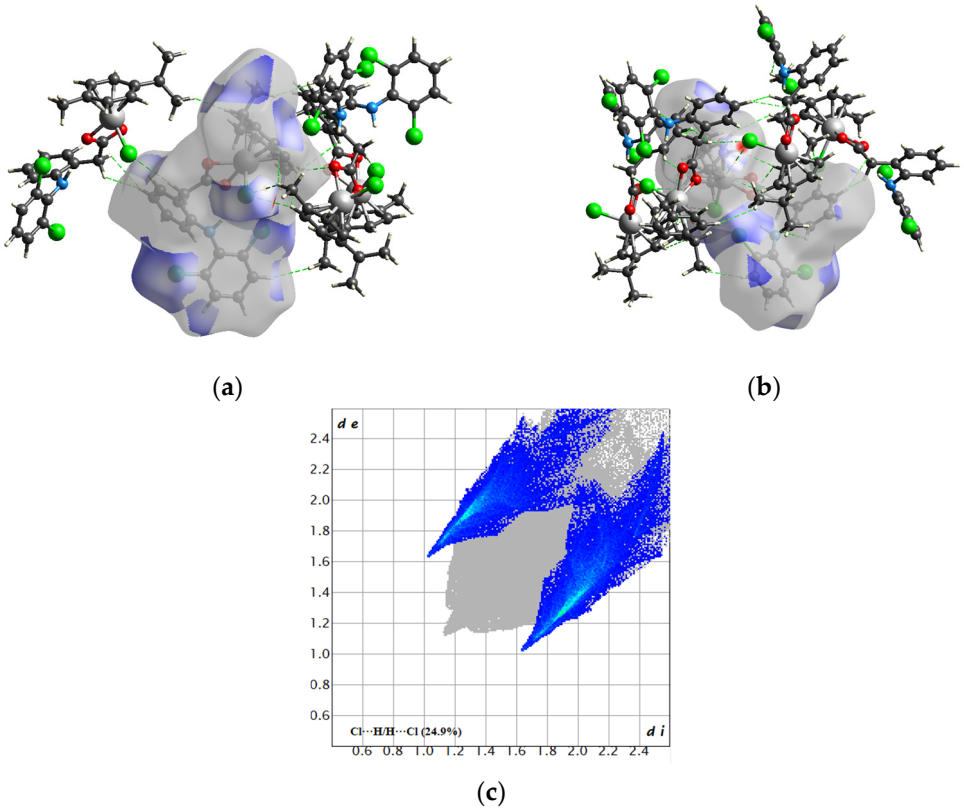

Figure 4. d_{norm} mapped Hirshfeld surface of the published complex [35] showing two views (**a**,**b**) on Cl···H/H···Cl close contacts with corresponding fingerprint plot (**c**).

The Hirschfeld 2D fingerprints were used for a more quantitative analysis of close contacts. The largest fraction of close contacts on the Hirshfeld surface is weak van der Waals interaction of H···H type. In the case of the triclinic complex, the percentage is 49.9%, and in the case of the orthorhombic, it is 51.0%. The HAR models of the structure have an equal fraction of this interaction, specifically 50.6%. Another significant close contact is the weak hydrogen bonds Cl···H/H···Cl, which account for 22.4% in the case of the triclinic polymorph of the complex and 24.9% in the case of the orthorhombic polymorph. The HAR models show the same proportion of these close contacts, specifically 21.7%. Weak C···H/H···C interactions account for 13.9% and 10.8% in the case of the triclinic and orthorhombic complexes, respectively. In the case of this close contact, we can also observe a minimal difference in the HAR models, exactly 13.1% for HAR1 and 13.0% for the others. Further weaker hydrogen bonding is revealed by the contribution of the O···H/H···O interaction, which has a value of 7.4% in the case of the triclinic structure along with its HAR models. In the case of the orthorhombic complex, this close contact accounts for 6.1%. The presence of the π-π stacking interactions can be demonstrated by the differential proportion of C···C close contacts. Structures in which the π-π stacking is not found have a value of these contacts in the interval 3.4–3.9%; on the contrary, in the orthorhombic polymorph, this value is higher, specifically 6.1%. A graph representing the individual percentages of close contacts at Hirshfeld surfaces is shown in Figure 3a. Fingerprints with significant-close contacts are illustrated in Supplementary Material (Figures S16–S26).

2.4. Interaction with DNA

The titration of the prepared complex with ct-DNA was monitored by UV-Vis spectroscopy. This method can elucidate whether the complex interacts with ct-DNA, can provide information on the mode of interaction, and also provides the binding constant. First, the spectrum of the complex was measured, where a maximum could be seen at a wavelength of 275 nm. Subsequently, the solution of ct-DNA with concentration 1.57×10^{-4} M

was added sequentially in 16 additions, up to a total added volume of 900 µL. The changes in the UV-Vis spectrum of the complex are shown in Figure 5. Initially, a rapid decrease in absorbance was observed, and later an increase was noted. There is a blue shift (hypsochromic) to lower wavelengths. Data obtained from the UV-Vis study are summarized in Table 2.

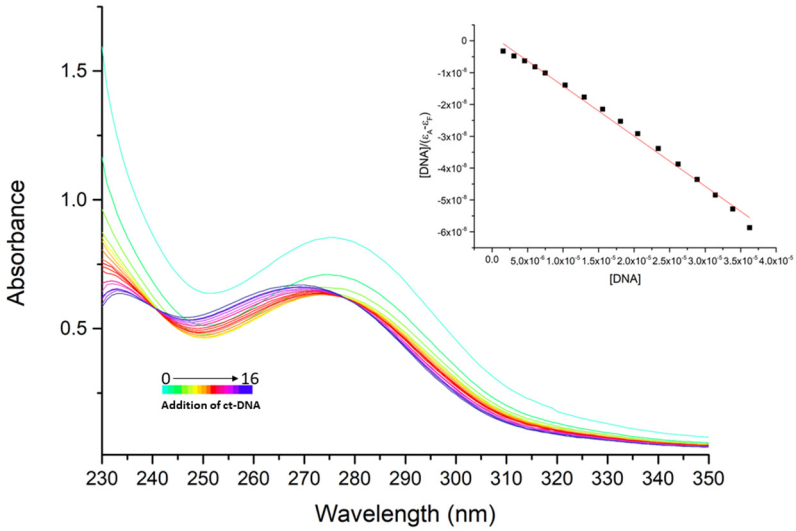

Figure 5. Changes in UV-Vis spectra of prepared complex due to increasing concentration of ct-DNA with Wolfe–Shimer plot of $[DNA]/(\varepsilon_A - \varepsilon_f)$ vs. [DNA].

Table 2. Data obtained from the UV-Vis study of interaction of prepared complex with ct-DNA.

λ (nm)	$\Delta\lambda$ (nm)	$\Delta A/A_0$ (%)	K_b (M^{-1})
275	−6	22 [a]	9.99 (±3.21) × 10^5
233	−1	49	5.35 (±0.61) × 10^5

[a] Due to the hyper- and hypochromism present, the first and last absorbance values were used to calculate the difference.

3. Materials and Methods

3.1. Materials and Synthesis

All chemicals and solvents used for synthesis were reagent grade (Acros Organics, Alfa Aesar, or Centralchem) and were used without further purification.

Synthesis of [Ru(p-cymene)(diclo)Cl]. To a 50 cm^3 of dichloromethane (DCM) solution of $[Ru_2(p\text{-cymene})_2Cl_4]$ (0.5 mmol, 0.306 g, 1 equiv.) 20 cm^3 of methanolic (MeOH) solution of diclofenac sodium salt (1 mmol, 0.318 g, 2 equiv.) was added. The reaction mixture was allowed to stir at laboratory temperature for two days. Subsequently, the solvent was removed using a rotary vacuum evaporator, and the solid was dissolved in 10 cm^3 of DCM. After filtration of the solution, a small amount of diethyl ether was added, and the solution was left to crystallize in the refrigerator in a sealed ampoule. After a few days, the product, in the form of orange crystals, was filtered out of the solution. The yield of the obtained product was 0.2582 g (46%). Elemental analysis for $[C_{24}H_{24}Cl_3NO_2Ru]$: exp. (calc.) (%) C 51.11 (51.03); H 4.25 (4.10); N 2.27 (2.48). FTIR (ATR) ν/cm^{-1}: 3286, 6066, 2956, 1721, 1562, 1506, 1442, 1388, 1272, 1088, 886, 776, 737, 695, 624, 450. ^1H NMR (300 MHz, $CDCl_3$, 298 K) δ/ppm: 7.32 [d, 2H, J = 8.0 Hz, CH of C_6H_4], 7.16 [d, J = 7.4 Hz 1H, CH of C_6H_4], 7.08 [m, 1H, CH of C_6H_4], 6.94 [m, 2H, CH of C_6H_4], 6.50 [d, 1H, J = 6.1 Hz, CH of C_6H_4], 5.60 [d, 2H, CH of p-cym], 5.38 [d, 2H, J = 6.1 Hz, CH of p-cym], 3.54 [s, 2H, CH_2 of CH_2COO], 2.86 [m, 1H, CH of $CH(CH_3)_2$], 2.27 [s, 3H, CH_3 of p-cym], 1.29 [m, 6H, CH_3 of $CH(CH_3)_2$].

3.2. Single-Crystal Crystallography

Data collection and cell refinement of all compounds were carried out using Stoe StadiVari diffractometer using Pilatus3R 300K HPAD detector. Xenocs Genix3D Cu HF (microfocused sealed tube, λ = 1.54186 Å) has been used as an X-ray source. The multi-scan absorption corrections were applied using the program Stoe LANA software [39]. The diffraction intensities were corrected for Lorentz and polarization factors. The structure was solved using ShelXT [40] program and refined by the full-matrix least-squares procedure Independent Atom Model (IAM) with ShelXL (version 2018/3) [41]. The structure of the complex was also refined by implementing Hirshfeld Atom Refinement (HAR) [42,43]. The NoSpherA2 implementation [44] of HAR makes used for tailor-made aspherical atomic factors calculated on-the-fly from a Hirshfeld-partitioned electron density. The least-squares refinements of the HAR model were then carried out with olex2.refine (version 1.5) [45]. The wave function for HAR was calculated using ORCA 4.2.0 software [46], hybrid exchange-correlation functional PBE0 [47]. For the purpose of comparison, the following relativistic basis sets were chosen: x2c-SVP (for HAR1); jorge-DZP-DKH (for HAR2); jorge-TZP-DKH (for HAR3); x2c-TZVP (for HAR4); and x2c-TZVPP (for HAR5) [48–50]. The following effective core potential (ECP) basis sets [51] were also chosen: ECP-def2-SVP (for HAR6); ECP-def2-TZVP (for HAR7); and ECP-def2-TZVPP (for HAR8) [52]. Geometrical analyses were performed with ShelXL/Olex2.refine. The structures were drawn with OLEX2 [53]. The crystal data, conditions of data collection, and refinement are reported in Table 3.

Table 3. Crystallographic data for the reported compound and for published polymorph [35].

Compound	***P*bca**	**1**
Chemical formula	$C_{24}H_{24}Cl_3NO_2Ru$	$C_{24}H_{24}Cl_3NO_2Ru$
Bases set	-(IAM)	-(IAM)
M_r	607.89	607.89
Crystal system	Orthorombic	Triclinic
Space group	*P*bca	$P\bar{1}$
T/K	298(2)	100
a/Å	16.8227(12)	9.4171(2)
b/Å	11.3329(8)	10.8706(2)
c/Å	25.1614(17)	12.7090(2)
α/°	90	90.2240(10)
β/°	90	107.2210(10)
γ/°	90	112.2920(10)
V/Å^3	4797.0(6)	1139.83(4)
Z	8	2
Crystal size/mm	0.36 × 0.27 × 0.24	0.11 × 0.063 × 0.03
ρ_{calc}/g·cm^{-3}	1.567	1.771
S	1.071	1.051
R_1 [$I > 2\sigma(I)$]	0.0282	0.0237
wR_2 [*All data*]	0.0741	0.0657
REFCODE/CCDC	TESSAO [35]	2235444

3.3. Hirshfeld Surface Analysis

The software CrystalExplorer (version 21.5) [54] was used to calculate the Hirshfeld surface [55,56] and associated fingerprint plots [57–63].

3.4. Spectral Methods

Infrared spectra were collected using NICOLET 5700 FTIR (Nicolet) spectrometer using the ATR technique at room temperature. UV-Vis spectra were measured on SPECORD 250 Plus (Carl Zeiss Jena). ^{1}H NMR spectrum was collected with Varian Unity-Inova (300 MHz). Chemical shifts are reported in ppm relative to $CDCl_3$ as an internal standard.

3.5. DNA Binding Studies

The interaction of the prepared complex with ct-DNA has been studied via the UV-Vis monitored titration. Firstly, the ct-DNA solution was prepared by dissolving in citrate buffer (containing 15 mM of sodium citrate and 150 mM of NaCl at pH = 7.0). Additionally, using the ratio of absorbance at 260 nm and at 280 nm, it was found that the ct-DNA was sufficiently pure from proteins [64]. The concentration of ct-DNA was determined by UV-Vis spectroscopy using the molar absorption coefficient of ct-DNA at 260 nm (6 600 $M^{-1}cm^{-1}$) [64]. The UV-Vis spectra of the prepared complex were collected in the presence of DNA at increasing concentrations. The DNA-binding constant of the complex, K_b (M^{-1}), was determined via the Wolfe–Shimer equation and the plot [DNA]/(ε_A-ε_f) vs. [DNA].

4. Discussion

The synthesis of the new polymorph of complex [Ru(p-cymene)(diclo)Cl] was based on a slightly different procedure than the one published [35] for orthorhombic polymorph, and the differences were also in the procedure of preparation of the single crystals. The composition and purity of the sample were confirmed using spectral methods, with results indicating slow hydrolysis of the complex. X-ray structural analysis revealed that it is a new polymorph, specifically the complex that crystallizes in a triclinic system with a $P\bar{1}$ space group. If we compare the impact of HAR on R_1 and wR_2 values (Table 2), we can say that there has been a decrease in these values compared to the non-aspheric refinement. Specifically, the closest to the model refined without HAR is model HAR2 with Douglas–Kroll–Hess Gaussian basis set with double zeta valence quality (Jorge-DZP-DKH). Next in order is the model HAR1, which is based on the Karlsruhe split valence polarization bases set. The best and, at the same time, very similar results were obtained using higher level bases sets, with triple-zeta polarisation (x2c-TZVP in HAR4, x2c-TZVPP in HAR5, and Jorge-TZP-DKH in HAR3). By comparing the bond lengths between the ruthenium(II) central atom and chlorido ligand, it can be concluded that the use of HAR resulted in a slight reduction in these lengths independent of the chosen basis set. Additionally, very small changes are observed in the case of ruthenium(II) and p-cymene centroid distance. In the case of bond lengths between the oxygen donor atoms of diclofenac and the central atom, a slight decrease is observed in one case, and a significant increase in the length of Ru1-O2 bonds is observed (Table 2). These differences are shown graphically in Figure 6.

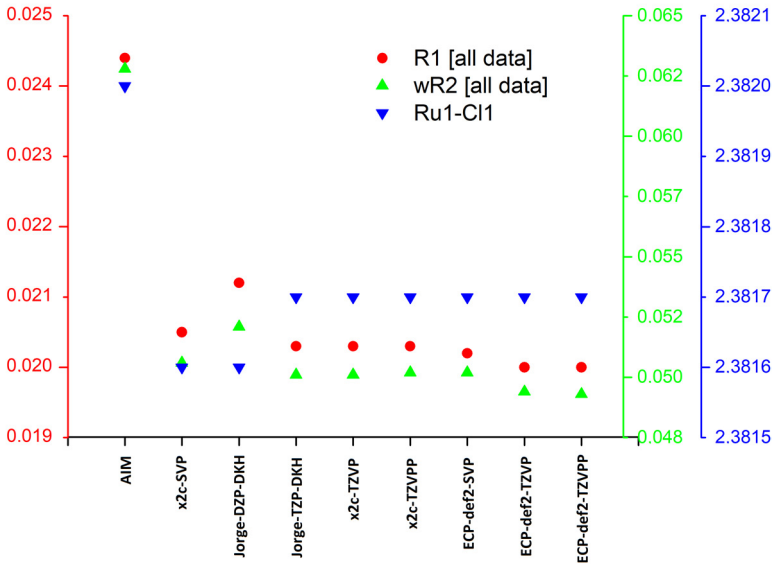

Figure 6. Graph showing the influence of HAR/IAM and the base used on the observed parameters of the crystal structures.

Analysis of the supramolecular structure of all the obtained models, together with the published polymorph, was performed using Hirshfeld surfaces. The analysis showed a significant difference between the polymorphs. It was also confirmed that the described changes in the molecular structures due to the HAR base were not significantly reflected in the supramolecular structure.

The interaction of the complex with ct-DNA was also studied using UV-Vis spectroscopy; also, Mandal et al. performed a study of the interaction of the complex with ct-DNA using fluorescence spectroscopy and found that the complex was unable to displace EB from the EB–DNA complex [35]. Based on this, they suggested that interaction with DNA is not the primary mechanism of the antiproliferative effects of the complex. Based on our study, it can be said that some interaction does occur (due to changes in spectrum with blue shift). The binding constant calculated according to the peak at 275 nm is equal to $K_b = 9.99 \times 10^5$ M^{-1}. However, this value is burdened with a significant error because of DNA absorption in this area. Therefore, it was also calculated according to the peak at 233 nm. This more accurate value is $K_b = 5.35 \times 10^5$ M^{-1}. However, we have not confirmed a clear mechanism of interaction either due to more complex changes in the spectrum.

Supplementary Materials: The following supporting information can be downloaded at: https://www.mdpi.com/article/10.3390/inorganics11050190/s1, Figure S1: The 1H NMR spectrum of prepared complex; Figure S2: The FTIR spectrum of prepared complex; Figure S3: Comparation of FTIR spectra of prepared complex and diclofenac sodium salt; Figure S4: Comparation of FTIR spectra of prepared complex and dimeric precursor; Figure S5: Hirshfeld surface for HAR1 model of complex mapped over d_{norm} (left) and shape index (right); Figure S6: Hirshfeld surface for HAR2 model of complex mapped over d_{norm} (left) and shape index (right); Figure S7: Hirshfeld surface for HAR3 model of complex mapped over d_{norm} (left) and shape index (right); Figure S8: Hirshfeld surface for HAR4 model of complex mapped over d_{norm} (left) and shape index (right); Figure S9: Hirshfeld surface for HAR5 model of complex mapped over d_{norm} (left) and shape index (right); Figure S10 Hirshfeld surface for HAR6 model of complex mapped over d_{norm} (left) and shape index (right); Figure S11 Hirshfeld surface for HAR7 model of complex mapped over d_{norm} (left) and shape index (right); Figure S12 Hirshfeld surface for HAR8 model of complex mapped over d_{norm} (left) and shape index (right); Figure S13 Hirshfeld surface for prepared complex with non-HAR (IAM) model of complex mapped over d_{norm} (left) and shape index (right); Figure S14 Hirshfeld surface for orthorhombic polymorph of complex mapped over d_{norm} (left) and shape index (right) [35]; Figure S15 Hirshfeld surface mapped over the electrostatic potential of 1 (top) and orthorhom-bic polymorph (botton), with positive and negative potential indicated in blue and red, respectively; Figure S16 The full two-dimensional fingerprint plots of prepared complex (AIM model), showing (a) all interactions, (b) O···H/H···O, (c) C···H/H···C, (d) C···C, (e) H···H, and (f) Cl···H/H···Cl close contacts; Figure S17 The full two-dimensional fingerprint plots of HAR1 model of pre-pared complex, showing (a) all interactions, (b) O···H/H···O, (c) C···H/H···C, (d) C···C, (e) H···H, and (f) Cl···H/H···Cl close contacts; Figure S18 The full two-dimensional fingerprint plots of HAR2 model of prepared complex, showing (a) all interactions, (b) O···H/H···O, (c) C···H/H···C, (d) C···C, (e) H···H, and (f) Cl···H/H···Cl close contacts; Figure S19 The full two-dimensional fingerprint plots of HAR3 model of prepared complex, showing (a) all interactions, (b) O···H/H···O, (c) C···H/H···C, (d) C···C, (e) H···H, and (f) Cl···H/H···Cl close contacts; Figure S20 The full two-dimensional fingerprint plots of HAR4 model of prepared complex, showing (a) all interactions, (b) O···H/H···O, (c) C···H/H···C, (d) C···C, (e) H···H, and (f) Cl···H/H···Cl close contacts; Figure S21 The full two-dimensional fingerprint plots of HAR5 model of prepared complex, showing (a) all inter-actions, (b) O···H/H···O, (c) C···H/H···C, (d) C···C, (e) H···H, and (f) Cl···H/H···Cl close contacts; Figure S22 The full two-dimensional fingerprint plots of HAR6 model of prepared complex, showing (a) all interactions, (b) O···H/H···O, (c) C···H/H···C, (d) C···C, (e) H···H, and (f) Cl···H/H···Cl close contacts; Figure S23 The full two-dimensional fingerprint plots of HAR7 model of prepared com-plex, showing (a) all interactions, (b) O···H/H···O, (c) C···H/H···C, (d) C···C, (e) H···H, and (f) Cl···H/H···Cl close contacts; Figure S24 The full two-dimensional fingerprint plots of HAR8 model of prepared complex, showing (a) all interactions, (b) O···H/H···O, (c) C···H/H···C, (d) C···C, (e) H···H, and (f) Cl···H/H···Cl close contacts; Figure S25 The full two-dimensional fingerprint plots of orthorhombic polymorph [35], showing (a)

all interactions, (b) O···H/H···O, (c) C···H/H···C, (d) C···C, (e) H···H, and (f) Cl···H/H···Cl close contacts; Figure S26 π-π interactions in a polymorph that was previously published [35].

Author Contributions: Conceptualization, J.M.; methodology, M.S. and M.P.; software, M.S. and J.M.; validation, M.S., K.L. and J.B.; formal analysis, M.S. and M.P.; investigation, M.S. and M.P.; resources, J.B.; data curation, K.L. and J.B.; writing—original draft preparation, M.S.; writing—review and editing, J.M.; visualization, M.S.; supervision, J.M.; project administration, J.M. All authors have read and agreed to the published version of the manuscript.

Funding: This work has been created with the support of the Ministry of Education, Science, Research, and Sport of the Slovak Republic within the Research and Development Operational Program for the project "University Science Park of STU Bratislava", ITMS 26240220084, co-funded by the Slovak Research and Development Agency under the contract No. APVV-19-0087 by the Scientific Grant Agency of the Slovak Republic (Project 1/0686/23).

Institutional Review Board Statement: Not applicable.

Informed Consent Statement: Not applicable.

Data Availability Statement: Not applicable.

Conflicts of Interest: The authors declare no conflict of interest.

References

1. Gan, T.J. Diclofenac: An update on its mechanism of action and safety profile. *Curr. Med. Res. Opin.* **2010**, *7*, 1715–1731. [CrossRef] [PubMed]
2. Sallman, A.R. The history of diclofenac. *Am. J. Med.* **1986**, *80*, 29–33. [CrossRef] [PubMed]
3. Vane, J.R.; Botting, R.M. Mechanism of action of nonsteroidal anti-inflammatory drugs. *Am. J. Med.* **1998**, *104*, 2S–8S. [CrossRef]
4. Srivastava, P.; Mishra, R.; Verma, M.; Sivakumar, S.; Patra, A.K. Cytotoxic ruthenium(II) polypyridyl complexes with naproxen as NSAID: Synthesis, biological interactions and antioxidant activity. *Polyhedron* **2019**, *172*, 132–140. [CrossRef]
5. Kumar, P.; Swagatika, A.; Dasari, S.; Tomar, R.S.; Patra, A.K. Modulation of ruthenium anticancer drugs analogs with tolfenamic acid: Reactivity, biological interactions and growth inhibition of yeast cell. *J. Inorg. Biochem.* **2019**, *199*, 110769. [CrossRef] [PubMed]
6. Kovala-Demertzi, D. Transition metal complexes of diclofenac with potentially interesting anti-inflammatory activity. *J. Inorg. Biochem.* **2000**, *79*, 153–157. [CrossRef]
7. Biswas, P.; Datta, H.K.; Dastidar, P. Multi-NSAID-based Zn(II) coordination complex-derived metallogelators/metallogels as plausible multi-drug self-delivery systems. *Chem. Commun.* **2022**, *58*, 969–972. [CrossRef]
8. Tarushi, A.; Hatzimitriou, A.G.; Estrader, M.; Kessissoglou, D.P.; Tangoulis, V.; Psomas, G. Toward multifunctional materials incorporating stepladder manganese(III) inverse-[9-MC-3[-metallacrowns and anti-inflammatory drugs. *Inorg. Chem.* **2017**, *56*, 7048–7057. [CrossRef]
9. Kumar, S.; Sharma, R.P.; Venugopalan, P.; Ferretti, V.; Perontsis, S.; Psomas, G. Copper(II) diclofenac complexes: Synthesis, structural studies and interaction with albumins and cald-thymus DNA. *J. Inorg. Biochem.* **2018**, *187*, 97–108. [CrossRef]
10. Perontsis, S.; Dimitriou, A.; Fotiadou, P.; Hatzidimitriou, A.G.; Papadopoulos, A.N.; Psomas, G. Cobalt(II) complexes with the non-steroidal anti-inflammatory drug diclofenac and nitrogen-donor ligands. *J. Inorg. Biochem.* **2019**, *196*, 110688. [CrossRef]
11. Bera, S.; Chowdhury, A.; Sarkar, K.; Dastidar, P. Design and synthesis of ZnII-coordination polymers anchored with NSAIDs: Metallovesicle formation and multi-drug delivery. *Chem. Asian J.* **2020**, *15*, 503–510. [CrossRef]
12. Lu, C.; Laws, K.; Eskandari, A.; Suntharalingam, K. A reactive oxygen species-generating, cyclooxygenase-2 inhibiting, cancer stem cell-potent tetranuclear copper(II) cluster. *Dalton Trans.* **2017**, *46*, 12785–12789. [CrossRef] [PubMed]
13. Garcia-Garcia, A.; Mendez-Arriaga, J.M.; Martin-Escolano, R.; Cepeda, J.; Gomez-Ruiz, S.; Salinas-Castillo, A.; Seco, J.M.; Sanchez-Moreno, M.; Choquesillo, A.; Ruiz-Muelle, A.B.; et al. In vitro evaluation of leishmanicidal properties of a new family of monodimensional coordination polymers based on diclofenac ligand. *Polyhedron* **2020**, *184*, 114570. [CrossRef]
14. Alisir, S.H.; Bariboga, B.; Caglar, S.; Buyukgungor, O. Synthesis, characterization, photoluminescent bproperties ant antimicrobial activities of two novel polymeric silver(I) complexes with diclofenac. *J. Mol. Struct.* **2017**, *1130*, 156–164. [CrossRef]
15. Mondal, S.; Dastidar, P. Designing metallogelators derived from NSAID-basef Zn(II) coordination complexes for drug-delivery applications. *Chem. Asian J.* **2020**, *15*, 3558–3567. [CrossRef]
16. Zampakou, M.; Tangoulis, V.; Raptopoulou, C.P.; Psycharism, V.; Papadopoulos, A.N.; Psomas, G. Structurally diverse manganese(II)-diclofenac complex showing enhanced antioxidant activity and affinity to serum albumins in comparison to sodium dichlofenac. *Eur. J. Inorg. Chem.* **2015**, *13*, 2285–2294. [CrossRef]
17. Sayen, S.; Carlier, A.; Tarpin, M.; Guillon, E. A novel copper(II) mononuclear complex with the non-steroidl anti-inflammatory drug diclofenac: Structural characterization and biological activity. *J. Inorg. Biochem.* **2013**, *120*, 39–43. [CrossRef]

18. Banti, C.N.; Jatzidimitriou, A.G.; Koirkoumelis, N.; Hadjikakou, S.K.; Tarpin, M.; Guillon, E. Diclofenac conjugates wuth biocides through silver(I) ions (CoMeD's); development of a reliable model for the prediction of anti-proliferation of NSAID's-silver formulations. *J. Inorg. Biochem.* **2019**, *194*, 7–18. [CrossRef]
19. Kakoulidou, C.; Gritzapis, P.S.; Hatzidimitriou, A.G.; Fylaktakidou, K.C.; Psomas, G. Zn(II) complexes of (E)-4-(2-(2-(pyridin-2-ylmethylene)hydrazinyl)quinazoline in combination with non-steroidal anti-inflammatory drug sodium diclofenac: Structure, DNA binding and photo-cleavage studies, antioxidant activity and interaction with albumin. *J. Inorg. Biochem.* **2020**, *211*, 111194. [CrossRef]
20. Caglar, S.; Aydernir, I.E.; Adiguzel, E.; Caglar, B.; Buyukgungor, O. Four copper(II) diclofenac complexes with pyridine derivatives: Synthesis, crystal structures, spectroscopic properties, thermal analysis and catechol oxidase activities. *Inorg. Chim. Acta* **2013**, *408*, 131–138. [CrossRef]
21. Biswas, P.; Dastidar, P. Anchoring drugs to a zinc(II) coordintion polymer network: Exploiting structural rationale toward the desigb if metallogels for drug-delivery applications. *Inorg. Chem.* **2021**, *60*, 3218–3231. [CrossRef] [PubMed]
22. Dos Santos, P.R.; Pitch, C.T.; Back, D.; Smiderle, F.; Dumas, F.; Moura, S. Synthesis, chemical characterization and DNA interaction study of new diclofenac and ibuprofen zinc(II)-nicotinamide ternary complexes as cyclooxygense inhibitor prototypes. *J. Inorg. Biochem.* **2020**, *206*, 111046. [CrossRef] [PubMed]
23. Ashouri, F.; Faraji, A.R.; Molaeian, S.; Fall, M.A.; Butcher, R.J. The novel cobalt and manganese polymeric complex with the non-steroidal anti-inflammatory drug diclofenac: Synthesis, characterization and antivacterial studies. *J. Mol. Struct.* **2020**, *1204*, 127483. [CrossRef]
24. Paul, M.; Sarkar, K.; Deb, J.; Dastidar, P. Hand-ground nanoscale ZnII-based coordination polymers derived from NSAIDs: Cell migration inhibition of human breast cancer cells. *Chem. Eur. J.* **2017**, *23*, 5736–5747. [CrossRef] [PubMed]
25. Johnson, A.; Iffland-Muhlhaus, L.; Northcote-Smith, J.; Singh, K.; Ortu, F.; Apfel, U.P.; Sunthealingam, K. A bioinspired redox-modulating copper(II)-macroxyclic complex bearing non-steroidal anti-inflammatory drugs with anti-cancer stem cell activity. *Dalton Trans.* **2022**, *54*, 5904–5912. [CrossRef]
26. Tarushi, A.; Raptopoulou, C.P.; Psychris, V.; Kontos, C.K.; Kessissoglou, D.P.; Scorillas, A.; Tangoulis, V.; Psomas, G. Copper(II) inverse-[9-metallacrown-3] compounds accommodating nitrato or diclofenac ligands: Structure, magnetism, and biological activity. *Eur. J. Inorg. Chem.* **2016**, *2*, 219–231. [CrossRef]
27. Altay, A.; Caglar, S.; Caglar, B.; Sahin, O. Synthesis, structural, thermal elucidation and in vitro anticancer activity of novel silver(I) complexes with non-steroidal anti-inflammatory drugs diclofenac and mefenamic acid including picoline derivatives. *Polyhedron* **2018**, *151*, 160–170. [CrossRef]
28. Alisir, S.H.; Dege, N.; Tapramaz, R. Synthesis, crystal structures and characterizations of three new copper(II) complexes including anti-inflammatory diclofenac. *Acta Crystallogr.* **2019**, *C75*, 388–397. [CrossRef]
29. Sayen, S.; Guillon, E. Tetra kis{2-[2-(2,6-dichloro anilino)phen yl]ethano ato-κ2O:O′}bis [(dimethyl sulfoxide-κO)copper(II)](Cu-Cu): A binuclear CuII complex with the non-steroidal anti-inflammatory drug diclofenac. *Acta Crystallogr.* **2012**, *E68*, m474–m475. [CrossRef]
30. Antonenko, T.A.; Gracheva, Y.A.; Shpakovsky, D.B.; Vorobyev, M.A.; Tafeenko, V.A.; Mazur, D.M.; Milaeva, E.R. Cytotoxic activity of organotin compounds containing non-steroidal anti-inflammatory drugs. *J. Organomet. Chem.* **2022**, *960*, 122191. [CrossRef]
31. Kourkoumelis, N.; Kovala-Demertzi, D.; Tiekink, E.R.T. Crystal and molecular structure of 1,2:3,4-di-μ2-[2,6-dichlorophenyl) amino]benzeneacetato-O,O-l,3-bis[(2,6-dichlorophenyl)amino]-benzeneacetato-O-1,2,4:2,3,4-di-μ3-oxo-tetrakis[di-n-butyltin(IV)]: {[$nBu_2Sn(O_2CCH_2C_6H_4N(H)C_6H_3Cl_2)]_2O$}$_2$. *Z. Kristallogr.* **1999**, *214*, 758–762. [CrossRef]
32. Li, S.-H.; Zhao, Y.; Zhang, L. Crystal structure of catena-poly-[(μ2-2-(2-((2,6-dimethylphenyl)amino)phenyl)acetato-κ2O:O′)(μ2-2-(2-((2,6-dimethylphenyl)amino)phenyl)acetate-κ3O,O′:O′)cadmium(II)]].$C_{28}H_{20}N_2Cl_4O_4Cd$. *Z. Kristallogr. NCS* **2016**, *231*, 1009–1011. [CrossRef]
33. Oliveira, K.M.; Honorato, J.; Gonçalves, G.R.; Cominetti, M.R.; Batista, A.A.; Correa, R.S. Ru(II)/diclofenac-based complexes: DNA, BSA interaction and their anticancer evaluation against lung and breast tumor cells. *Dalton Trans.* **2020**, *49*, 12643–12652. [CrossRef] [PubMed]
34. Khan, R.A.; Al-Lohedan, H.A.; Farah, M.A.; Ali, M.S.; Alsalme, A.; Al-Anazi, K.M.; Tabassum, S. Evaluation of (η6-p-cymene) ruthenium diclofenac complex as anticancer chemotherapeutic agent: Interaction with biomolecules, cytotoxicity assays. *J. Biomol. Struct. Dyn.* **2019**, *37*, 3905–3913. [CrossRef]
35. Mandal, P.; Kundu, B.K.; Vyas, K.; Sabu, V.; Helen, A.; Dhankar, S.S.; Nagaraja, C.M.; Bhattacherjee, D.; Bhabak, K.P.; Mukhopadhyay, S. Ruthenium(II) Arene NSAID Complexes: Inhibition of cyclooxygenase and antiproliferative activity against cancer cell lines. *Dalton Trans.* **2018**, *47*, 517–527. [CrossRef]
36. Nakamoto, I. *Infrared and Raman Spectra of Inorganic and Coordination Compounds, Part B*, 6th ed.; Wiley: Hoboken, NJ, USA, 2009.
37. Janiak, C. A critical account on π-π stacking in metal complexes with aromatic nitrogen-containing ligands. *J. Chem. Soc. Dalton Trans.* **2020**, *21*, 3885–3896. [CrossRef]
38. Spackman, M.A.; McKinnon, J.J.; Jayalitaka, D. Electrostatic potentials mapped on Hirshfeld surfaces provide direct insight into intermolecular interactions in crystals. *Cryst. Eng. Comm.* **2008**, *10*, 377–388. [CrossRef]
39. Koziskova, J.; Hahn, F.; Richter, J.; Kožíšek, J. Comparison of different absorption corrections on the model structure of tetrakis(μ2-acetato)-diaqua-di-copper(II). *Acta Chim. Slovaca* **2016**, *9*, 136–140. [CrossRef]
40. Sheldrick, G.M. SHELXT–Integrated space-group and crystal-structure determination. *Acta Crystallogr.* **2015**, *A71*, 3–8. [CrossRef]
41. Sheldrick, G.M. Crystal structure refinement with SHELXL. *Acta Crystallogr.* **2015**, *C71*, 3–8. [CrossRef]

42. Capelli, S.C.; Bürgi, H.-B.; Dittrich, B.; Grabowsky, S.; Jayatilaka, D. Hirshfeld atom refinement. *IUCrJ* **2014**, *1*, 361–379. [CrossRef] [PubMed]
43. Chrappová, J.; Pateda, Y.R.; Rakovský, E. Molecular acidity: Synthesis and crystal structure analysis of $NH_4[Zn(cma)(H_2O)_2]\cdot H_2O$ using IAM and HAR approaches. *J. Chem. Crystallogr.* 2022; *in press*. [CrossRef]
44. Kleemiss, F.; Dolomanov, O.V.; Bodensteiner, M.; Peyerimhoff, N.; Midgley, L.; Bourhis, L.J.; Genoni, A.; Malaspina, L.A.; Jayatilaka, D.; Spencer, J.L.; et al. Accurate crystal structures and chemical properties from NoSpherA2. *Chem. Sci.* **2021**, *12*, 1675–1692. [CrossRef] [PubMed]
45. Bourhis, L.J.; Dolomanov, O.V.; Gildea, R.J.; Howard, J.A.K.; Puschmann, H. The anatomy of a comprehensive constrained, restrained refinement program for the modern computing environment—Olex2 dissected. *Acta Crystallogr.* **2015**, *A71*, 59–75. [CrossRef]
46. Neese, F. Software update: The ORCA program system, version 4.0. *WIREs Comput. Mol. Sci.* **2018**, *8*, e1327. [CrossRef]
47. Adamo, C.; Barone, V. Toward reliable density functional methods without adjustable parameters: The PBE0 model. *J. Chem. Phys.* **1999**, *110*, 6158–6169. [CrossRef]
48. Pollak, P.; Weigend, F. Segmented contracted error-consistent basis sets of double- and Triple-ζ valence quality for one- and two-component relativistic all-electron calculations. *J. Chem. Theory Comput.* **2017**, *13*, 3696–3705. [CrossRef]
49. Barros, C.L.; de Oliveira, P.J.P.; Jorge, F.E.; Canal Neto, A.; Campos, M. Gaussian basis set of double zeta quality for atoms Rb through Xe: Application in non-relativistic and relativistic calculations of atomic and molecular properties. *Mol. Phys.* **2010**, *108*, 1965–1972. [CrossRef]
50. Campos, C.T.; Jorge, F.E. Triple zeta quality basis sets for atoms Rb through Xe: Application in CCSD(T) atomic and molecular property calculations. *Mol. Phys.* **2013**, *111*, 167–173. [CrossRef]
51. Andrae, D.; Häußermann, U.; Dolg, M.; Stoll, H.; Preuß, H. Energy-adjustedab initio pseudopotentials for the second and third row transition elements. *Theor. Chim. Acta* **1990**, *77*, 123–141. [CrossRef]
52. Weigend, F.; Ahlrichs, R. Balanced basis sets of split valence, triple zeta valence and quadruple zeta valence quality for H to Rn: Design and assessment of accuracy. *Phys. Chem. Chem. Phys.* **2005**, *7*, 3297. [CrossRef]
53. Dolomanov, O.V.; Bourhis, L.J.; Gildea, R.J.; Howard, J.A.K.; Puschmann, H. OLEX2: A complete structure solution, refinement and analysis program. *J. Appl. Crystallogr.* **2009**, *42*, 339–341. [CrossRef]
54. Spackman, P.R.; Turner, M.J.; McKinnon, J.J.; Wolff, S.K.; Grimwood, D.J.; Jayalitaka, D.; Spackman, M.A. CrystalExplorer: A program for Hirshfeld surface analysis, visualization and quantitative analysis of molecular crystals. *J. Appl. Crystallogr.* **2021**, *54*, 1006–1011. [CrossRef] [PubMed]
55. Hirshfeld, F.L. Vobded-atom fragments for describing molecular charge densities. *Theor. Chim. Acta.* **1977**, *44*, 129–138. [CrossRef]
56. Spackman, M.A.; Jayalitaka, D. Hirhfeld surface analysis. *Cryst. Eng. Comm.* **2009**, *11*, 19–32. [CrossRef]
57. Spackman, M.A.; McKinnon, J.J. Fingerprinting intermolecular interactions in molecular crystals. *Cryst. Eng. Comm.* **2002**, *4*, 378–392. [CrossRef]
58. Parkin, A.; Barr, G.; Dong, W.; Gilmore, C.J.; Jayalitaka, D.; McKinnon, J.J.; Spackman, M.A.; Wilson, C.C. Comparing entire crystal structures: Structural genetic fingerprinting. *Cryst. Eng. Comm.* **2007**, *9*, 648–652. [CrossRef]
59. McKinnon, J.J.; Jayalitaka, D.; Spackman, M.A. Towards quantitative analysis of intermolecular interactions with Hirshfeld surfaces. *Chem. Commun.* **2007**, 3814–3816. [CrossRef]
60. Wang, K.; He, X.; Rong, C.; Zhong, A.; Liu, S.; Zhao, D. On the origin and nature of internal methyl rotation barriers: An information-theoretic approach study. *Theor. Chem. Acc.* **2022**, *141*, 68. [CrossRef]
61. Liu, S.; Pederse, L.G. Estimation of Molecular Acidity via Electrostatic Potential at the Nucleus and Valence Natural Atomic Orbitals. *J. Phys. Chem. A* **2019**, *123*, 6751–6760. [CrossRef]
62. Cao, X.; Rong, C.; Zhong, A.; Lu, T.; Liu, S. Molecular acidity: An accurate description with information-theoretic approach in density functional reactivity theory. *J. Comput. Chem.* **2018**, *39*, 117–129. [CrossRef]
63. Marmur, J. Thermal renaturation of deoxyribonucleic acids. *J. Mol. Biol.* **1961**, *3*, 208–211. [CrossRef]
64. Reichmann, M.F.; Rice, S.A.; Thomas, C.A.; Doty, P.J. A Further Examination of the Molecular Weight and Size of Desoxypentose Nucleic Acid. *J. Am. Chem. Soc.* **1954**, *76*, 3047–3053. [CrossRef]